The Photocatalytic Rate of ZnO Supported Onto A Natural Zeolite Nanoparticles In The Photodegradation of An Aromatic Amine

Fereshteh Iazdani
Islamic Azad University
Alireza Nezamzadeh-Ejhieh (arnezamzadeh@iaush.ac.ir)
Islamic Azad University https://orcid.org/0000-0002-8123-6968

Research Article

Keywords: ZnO, Apparent first order Hinshelwood kinetic, Dichloroaniline, Clinoptilolite, Heterogeneous photocatalysis

Posted Date: April 19th, 2021

DOI: https://doi.org/10.21203/rs.3.rs-300323/v1

Abstract

The ZnO supported on the ball-mill prepared clinoptilolite nanoparticles (CNPs) was prepared via an ion-exchange process followed by the calcination process. The ZnO-CNP catalyst was briefly characterized by XRD, FTIR, and DRS techniques. The pHpzc value for the various ZnO-CNPs was about 7.1 that no changed with the ZnO loading. By applying the Scherrer equation on the XRD results, a nano-dimension was obtained for the catalyst. Band gap energy of the ZnO-CNP samples were estimated by applying the Kubelka-Munk equation on the DRS reflectance spectra. The supported ZnO-CNP sample was then used in the photodegradation of 2,4-dichloroaniline (DCA).The effects of the most important key operating factors on the degradation efficiency was kinetically studied by applying the Hinshelwood equation on the results. The ZnO-CNP catalyst with 2 w% ZnO showed the best photocatalytic rate in the optimal conditions of 0.75 g/L, C_{DCA}: 15 ppm, and the initial pH: 5.8. Finally, HPLC analysis of the blank and the photodegraded DCA solutions at 180 and 300 min confirmed 74 and 87% of DCA molecules were degraded during these times.

Introduction

Nowadays, an increased need to purified water is essential for the human's life due to the increased world population and industrial activities. The increased industrial activities drastically polluted the aquatic resources due to the discharge of the wastewater into the environment. In contrast, such industrial activities are essential for human life. The increase in the world population needs also to an increased health and care activities and drugs. Unfortunately, there are no balances between these activities and the increased world population and thus the pollution of water supplies is major global problem at this time (Segundo et al. 2019; Ahmad Bhat et al. 2020; Huang et al. 2019)

An important class of chemicals with wide applications in pharmacological, biological and industrial activities is anilineand anilinederivates.These chemicals have adopted wide uses for manufacturing of pesticides, dyes, cosmetics,medicines, synthetic polymers, rubber, etc.These also used intermediates for preparing of many chemical compounds)Rappoport 2007 ; Akyuz et al. 2006). Thus, high amounts of these aromatic amines have been discharged into the aquatic environments resulting in a high pollution of the water resources. Aromatic amines have known as high toxic and carcinogenic agentsfor body life)Akyuz et al. 2006). The absorbed chloroanilines and chloroaminevia inhalation, ingestion or cutaneous cause thevertigo, headache, cyanosis, mental confusion deceases. This also causesanorexia, anemia, weight loss and cutaneous lesions as somechronic toxicities (Pande et al. 2011) .2,4-dichloroaniline (DCA) is the degradation product of some herbicides which is also known as a pollutant agent for the environment (Pande et al. 2011; Zh et al.2009).

Thus, the need of an ecofriendly removal method for removing such pollutants is of a great attention of environmental engineering and human health. This ecofriendly, cheap, and effective method is semiconducting based photocatalysis in which four main reactive species are responsible for destroying the organic pollutant from water. The initial photogenerated electron/hole pairs (e/h) can produce by the

illumination of arrived UV or visible photons in the conduction (CB) and valence (VB) of the semiconductor. These photoinduced e/h pairs can attack to the organic pollutants directly.They can also react with the dissolved oxygen and water molecules and produce superoxide and hydroxyl radicals, respectively, as other two main reactive species for destroying the pollutants (Habibi et al. 2011; Shabani et al. 2016; Honarmand et al. 2020; Khanmohammadi et al. 2020; Shah et al. 2016; Mohamed JafferSadiq et al. 2014; Rashmi et al. 2020; Bordbar et al. 2016).

Unfortunately, recombination of these e/h pairs drastically decreases the overall efficiency of a typical heterogeneous photodegradation catalysis. This can be overcame by various technologies such as doping of metals and not-metals into the semiconducting material, use the catalysts with nano-dimension, coupling of two or more semiconductors, supporting the catalyst into supports, the use of plasmonic systems, etc. Detailed mechanism pathways for these technologies have been illustrated in the literature (Vafayi et al. 2015; Palma et al. 2020; Rostami-Vartooni et al. 2019; Giahi et al. 2016; Naderpour et al. 2013; Pouretedal et al. 2017; Derikvandi et al. 2017; Bordbar et al. 2015; Derikvandi et al. 2020; Khodadadi et al. 2016; Pouretedal et al. 2016; Thirumalai et al. 2016).

In this work, for enhancing the photocatalytic activity of ZnO, it was supported on the clinoptilolitenano-particles (CNP). Generally zeolites have an internal electric field which helps to the prevention of the photogenerated e/h pairs in the photoexcited supported semiconductor (Behin et al. 2019; Divband et al. 2019; Rahimi et al. 2019). The n-type ZnOsemiconductor is a highly transparent material that has a band gap energy of about 3.3 eV for the direct electronic transition. It also has an exciton binding energy of about 60 meV (Matei et al. 2012) .Accordingly, it is a transparent material in the wavelength between 400 and 800 nm. This transparency can change by some techniques such as the doping of the various atoms (Yuonesi et al. 2010).

The supported ZnO-CNP was used in the photodegradation of 2,4-dichloroaniline (DCA). The catalysts was briefly characterized and used for the study of the kinetics of the photodegradation process. For this goal, Hinshelwood equation was applied on the results and the kinetics of some important experimental variables supporting effect, the size of clinoptilolite used, the amount of the loaded ZnO, solution pH, concentration of DCA and the dose of the ZnO-CNP catalyst was studied on the DCA photodegradation.

Experimental

2.1. Materials and preparations

Clinoptiloliteas a Semnanian natural tuff (from the north-east of Iran) was obtained Afrandtooska Co. (Iran). 2,4-dichloroaniline (DCA),HCl, HF, H_2SO_4, NaOH, HNO_3, NaCl, $Zn(NO_3)_2.6H_2O$, and other required chemicals were purchased from Merck. The chemicals had an analytical grade purity and their solutions were prepared in distilled water. The pH of solutions adjusted by NaOH or HCl solution.

The natural clinoptilolite tuff was changed into the micronized (CP) and nano(CNP) particles by the mechanical ball-mill method. Detailed procedures applied for pretreating of the obtained powders in

removal of the magnetic and water soluble impurities have been illustrated in the literature (Faghihian et al. 2008; Arabpour et al. 2015).

For preparing the ZnO-CNP sample, the experiments were carried out as below. About 0.5 g CNP sample was added to the closed bottle containing 10 mL 0.1 M Zn(II) solution and shaken for 24 h to complete the ion exchange process. After the separation of the solid powder by the centrifugation at 13000 rpm, it was washed many times with water and then dried in air. The dried powder was calcined at 450°C for 12 h to obtain the ZnO-CNP sample. A similar procedure was used for the preparation of ZnO-CP or ZnO-CNP sample with other Zn(II) concentrations.

2.2. Characterization methods

Fourier transformation infrared (FT-IR) spectra of the samples, were obtained with a Nicolet FT-IR (Impact 400D) spectrometer by using KBr pellets. The X-ray diffraction patterns for the samples were obtained by using a diffractometerBruker, D8ADVANCE, X-ray tube anode: Cu-Kα wavelength: 1.5406 Å, Filter: Ni. Diffuse reflectance spectra (DRS) of the samples were also obtained using JASCO V-670 (JASCO Co. Japan) equipped with an integrating sphere andan Hg lamp (75W) as the UV light source. The absorption spectra of DCA solutions wererecorded on a double beam spectrophotometer (Varian Carry 100 Scan).

HPLC chromatograms of DCA solutions were recorded by an Agilent Techonologies 1200 Series instrument with Quaternary pump, column XDB-C18 (length = 15 cm, internal diameter = 4.6 mm and particle size = 5 mm) and a UV detector. An atomic absorption spectrometer (AAS) 121 PerkinElmer Analyst (Air-C_2H_2, λ = 213.9 nm) was used for the quantitative determination of Zn in the catalysts. For this goal, the solid catalyst was digested in HF, $HClO_4$ and $HNO_3$and the resulted solution was introduced to the AAS instrument (Nosuhi et al. 2018; Sharifian et al. 2016).

2.3. Photodegradation experiments

To achieve an equilibrated adsorption/desorption process, the suspensions were shaken at dark for 10min before the irradiation process. In atypical photodegradation process, 10 mLDCA aqueous suspension (15 mg/L DCAat pH 5.8 containing 0.75 g/Lof the catalyst)in a 25 mL quartz beakerwas irradiated by a 35 W Hg-lamp on a magnetic stirrer. At definite times, the suspension was sampled out and centrifuged(> 13000 rpm). The absorbance of the supernatant (Ao for before and A for after irradiation process) was recorded at λ_{max} = 290 nm.The recorded absorbance values were then used for the calculation of degradation percent of DCA by the following equation:

$$\text{Degradation } \% = 100 \times \frac{(Ao - A)}{Ao} \qquad (1)$$

Results And Discussion

3.1. Characterization results

3.1.1. Determination of loaded ZnO in the prepared ZnO-CNP catalysts

The used ZnO-CNP catalysts prepared in this work are listed in Table 1. The chemical composition of the samples is summarized in this table, which shows that with increase in the Zn(II) concentration in solution the amount of Zn(II) loaded in CNP ion-exchange sites was relatively increased. The photodegradation experiments (see next sections) showed that the best photodegradation rate can be achieved by CZ2 catalyst. Thus, this catalyst was applied for characterization methods.

Table. 1. Chemical analysis of the ZnO-CNP catalysts.

Catalysts	$C_{Zn(II)}$ (in ion-exch. sol. (M))	Loaded Zn(II)	
		meq/g	ZnO%
CZ2: $ZnO_{2.0\%}$-CNP	0.1	0.54	2.0
CZ2.6: $ZnO_{2.6\%}$-NCP	0.2	0.63	2.6
CZ3: $ZnO_{3.0\%}$-CNP	0.3	0.72	3.0
CZ3.5: $ZnO_{3.5\%}$-CNP	0.5	0.86	3.5

3.1.2. Crystallite phase purity studies

The diffraction patterns of some CZ samples are shown in Fig. 1. In all patterns, the diffraction peaks of clinoptilolite have obviously appeared because it consists of majority of the samples. These peaks agree with the standard pattern according to JCPDS No. 39-1383 which assigned in the literature (Olad et al. 2011). Based on literature (Muhammad et al. 2019; Bindu et al. 2014), the hexagonal wurtzite phase of ZnO shows typical XRD peaks at 2θpositions of 31.8355°, 34.5207°, 36.2871°, 47.5808°, 56.6487°, 62.8917°, 66.4115°, 67.9331°, 69.1842° and 77.0106° according to JCPSD card no. 01-007-2551. These diffraction peaks correspond to the *hkl* Miller indices of (100), (002), (101), (102), (110), (103), (200), (112), (201), and (202), respectively.Here, XRD peaks of ZnO are weak due to the low weigh percentage of ZnO in the sample. Besides, some peaks have overlapped with those of clinoptilolite. Some important peaks of ZnO have assigned to the corresponding *hkl* planes. Finally, the average crystallite size of CZ samples was obtained below 50 nm by applying the Scherrer equation on the results (Arunkumar et al. 2020; Aghdasi et al. 2016).

3.1.3. FT-IR study

FT-IR spectra of the raw CNP and the ZnO-loaded CNP samples are shown in Fig. 2. The main peak positioned at 1092 cm^{-1} belongs to the Si-O-Si asymmetric stretching vibration. This peak usually appear in FTIR spectra of all zeolitic structures and its position changes depending on the Si/Al ratio of framework. Further, this peak overlaps with the Al-O-Si and Al-O stretching vibration modes. Here, some slight shifts in the range of 1082-1074 cm^{-1} appeared for the loaded CZ samples. Besides, the tetrahedra and double rings 4 and 6 atoms tetrahedral of the zeolite showed typical absorption peaks for stretching vibrations at 804-616 cm^{-1} and 476 cm^{-1}, respectively (Shahwan et al. 2005). In the ZnO-loaded samples,

the absorption peak at 804 cm^{-1} was shifted in the range of 797 to 795 cm^{-1}, while the peak at 616 cm^{-1} in the range of 610 to 602 cm^{-1}.

It has reported that the Zn-O bond can show FTIR absorption peak in the range of 500 to 400 cm^{-1} (Nagaraju et al. 2017). For example, the non-calcinedZnO sample showed a Zn-O absorption peak at about 457 cm^{-1}which shifted and splitted to 518 $cm^{-1}$and 682 cm^{-1} when calcined at 300 and 500 °C, respectively (SowriBabu et al. 2013). Here, the absorption peak of ZnO overlapped with the peak of zeolite at 476 cm^{-1} and caused to the broadening of the peak and slight shifts in the range of 482 to 474 cm^{-1}.

3.1.4. Estimation of pHpzc of ZnO-CNP

The accumulated charge on the surface of the catalyst plays a vital role in the efficiency of the proposed catalyst. On the other hand, the net charge present on the surface of the catalyst affects the adsorbed pollutant molecules on the surface, where hydroxyl, superoxide and other reactive species formed. The most important point for the evaluation of surface charge of the catalyst is the point of zero charge pH (pHpzc) in which the accumulated charge on the surface is neutralized by the surrounding solution. The method used for the determination of this pH has been illustrated in the literature (Eslami et al. 2018; Nezamzadeh-Ejhieh et al. 2014). Briefly, the suspensions of ZnO-CNP sample in 0.01 M NaCl solution (as the ionic strength buffer) were prepared and the pH was adjusted between 2 to 12 (pH_I: initial pH). After 24 h shaking, the final pH (pH_F) was recorded. Based on the results, two plots were constructed for the estimation of pHpzc of the sample (Fig. 3). Fig. 3A shows the bisector method, in which the plot of pH_I versus pH_I gives the bisector of the plot. The crossing point of the plot of pH_F versus pH_I gives the pHpzc for the sample. Fig. 3B shows the plot of ΔpH versus pH_I in which when ΔpH is zero, the crossing point of the curve with x-axis gives the pHpzc value for the sample.

As shown in Fig. 3A, the initial pHs of 2, 4, and 6 increased to about of 4.75. 6.63, and 6.93 after shaking with the catalysts. Accordingly, in ΔpH curve, the positive values obtained. ThesepHs located below pHpzc values. In these pHs the surface of the catalyst has negatively charged due to the adsorption of protons from the contacted aqueous solution. This process occurs due to the native negatively charged of the surface or its native basic property at such pHs. After the pHpzc, the native positively charged surface or its native acidic property caused to adsorption of hydroxyl anions from the adjacent aqueous solution and thus the surface got a net negatively charge. At such condition due to decrease in the concentration of hydroxyl anions in the solution, the pH of the adjacent solution was decreased. Thus the initial pHs of 8, 10, and 12 were changed to 7.08, 7.25, and 11, respectively. Accordingly, in ΔpH curve, the negative values obtained.The pHpzc point is a point in which the native basic property of the surface tend to change to the acidic property. Thus the curve crosses the bisector of the plot (Omrani et al. 2019; Yousefi et al. 2020).

Here, all samples have the pHpzc value about 7.1 (or 7.2) which confirms that this value has not affected by the amount of ZnO loaded on the surface.

3.1.5. DRS analysis

Some prepared CZ samples were subjected to diffuse reflectance spectroscopy (DRS) to study the energy required for carrying out the electronic transitions in the samples (or estimate the band gap energy). The obtained reflectance spectra are shown in Fig. 4A which used for further investigations by the Kubelka-Munk equation and Tauc plots. In theKubelka-Munk model (Eq. 2), the absolute reflectance (R) in the reflectance spectra should be changed to the transformed values (K). Then the obtained K-values should be changed to the Tauc equation (Eq. 3) by the procedures defined in the literature (Sobhani-Nasab et al. 2020; Azimi et al. 2015).

$K=(1-R)^2/2R$ (2)

$(\alpha h\upsilon)=\beta(h\upsilon-Eg)^n$ (3)

In equation 3, the band gap energy (Eg) for various electronic transitions (depending on the n-values) can be estimated by plots of $(\alpha h\upsilon)^n$ versus photon energy ($h\upsilon$). When the n-values of 1/2 and 2 use, the band gap energy of the allowed direct and indirect electronic transitions can be estimated, respectively. But, when the n-values of 3/2 and 3 substituted in equation 3, the Eg-values for the forbidden direct and indirect transitions can be estimated by the corresponding plots, respectively.In this equation, 'α' shows the absorption coefficient of the sample which varies with the change in sample transmission (T) and thickness (t) (1/t=ln (1/T)) (Dianat 2018; Balakrishnan et al. 2020; Ng Y-C 2011).

Typical Tauc plots for the various electronic transitions of the samples are shown in Fig. 4B-E. The rising slopes of the curves were extrapolated toward the x-axis. The crossing point shows the Eg-value for the investigated sample. The results are summarized in Table 2. As the results show, a slight shift in Eg-values was observed by change in the amount of ZnO loaded onto CNP.

Table 2. Band gap energies obtained for CuO-CNP samples with various CuO-loadings obtained by Kubelka-Munc theory and Tauc plots.

Catalysts	Band gap energy (eV) for n-vales of:			
	1/2	3/2	2	3
CZ2	3.16	3.79	3.64	3.88
CZ3	3.24	3.87	3.71	3.94
CZ3.5	3.21	3.85	3.68	3.97

3.2. Photodegradation results

3.2.1. Theory of the photodegradation kinetics

Here, the effects of the influencing variables were evaluated kinetically. Thus, the theory of the kinetics of a typical heterogeneous photodegradation catalysis will study here. The best model for this goal is the Langmuir-Hinshelwood (L-H) model which is constructed based on amonolayer adsorption of both the pollutant and the oxidant by the catalyst surface. The formation of this monolayer at the solid-liquid interface controls the rate of the overall process. On the other hand the formation of this monolayer is a key factor and is the rate-limiting step of the process.

General L-H model is shown by equation4 in which the most important factors in the reaction rate (r: in mg/L min) are the specific reaction rate constant (k: in mg/L min),the equilibrium constant of the reactant (K: in L/mg), and the concentration of the pollutant (C).When concentrations above 5 mM use, a zero order model is supposed, but at concentrations below mM an apparent first-order reaction is supposed.

$$r = -dC/dt = (k'KC)/(1+KC) = k'\theta \qquad (4)$$

Commonly, to simplify this equation its integratedor the logarithmic form has been used that shown by equation 5.In this apparent first-order equation,the initial concentration of the pollutant (C_o)changes to concentration at time t (C_t) by proceeding the photodegradation process.Thus,the constant k callsthe apparent first-order rate constant (DharmrajKhairnar et al. 2018; Assi et al. 2017; Mohammadi et al. 2020; Ghattavi et al. 2019).

$$\ln(C_o/C) + k'(C_o-C_t) = k'Kt = k \times t \qquad (5)$$

In the next section the kinetics of the effects of some important experimental variables will discuss.

3.2.2. The effects of clinoptilolite, ZnO supporting and loaded-ZnOamount

Fig. 5A shows typical Hinshelwood plots obtained in the DCA removal by the supported ZnO onto clinoptilolite comparing the unsupported one. The slopes of these curves as a measure of the apparent first-order rate constants of the DCA removal are summarized in Table 3. As mentioned in section 2.3, before the photodegradationexperiments, the suspension were shaken at dark for 10 min to remove the effects of the surface adsorption in DCA removal. Thus, the next photodegaradtion results will obtain and report in the next sections. A slight photodegradation efficiency was obtained by the raw CP and CNP. As we know, all zeolitic frameworks contain high amounts of AlO_4 and SiO_4tetrahedra. Thus their SiO_2 and Al_2O_3 unites act as semiconducting materials that can be excited against the arrived photons for the production of e/h pairs and the above-mentioned reactive radicals. When both CP and CNP ion-exchanged in Zn(II) solution, the resulted Zn(II)-CP and Zn(II)-CNP showed relatively faster rates in DCA photodegradation concerning the raw zeolites. In this case, some weak Zn-O bondsformed in the ion exchange sites of clinoptilolite that act as weak semiconductors.

Table 3. Rate-constant values in the photodegradation of DCA as the function of experimental variables.

Variables	Abbreviation	Value	$-k \times 10^{-3}$ (min^{-1})	
Effect of the supporting	**CP**	-	0.48	0.9741
	CNP	-	0.51	0.9908
	Zn/CP	-	0.53	0.9841
	Zn/CNP	-	0.61	0.9868
	Bulk ZnO	-	0.81	0.9796
	ZnO/CP		1.1	0.9963
	ZnO/CNP		**1.2**	**0.9796**
ZnO-loaded	**CZ2**	-	**1.20**	**0.9659**
	CZ2.6	-	1.07	0.9480
	CZ3	-	1.16	0.9665
	CZ3.5	-	1.27	0.9899
C_{DCA} (mg/L)		5	1.17	0.9743
		15	**1.50**	**0.9780**
		25	1.03	0.9901
		35	0.75	0.9782
Catalyst dose (g/L)	-	0.5	1.49	0.9659
	-	**0.75**	**1.83**	**0.9791**
	-	1	1.23	0.9830
pH	-	3	0.9	0.9451
	-	5	1.57	0.9331
		5.8	**1.86**	**0.9558**
		7	1.52	0.9682
		10	1.11	0.9484

When the calcinedZnO-zeolite samples were used the photodegradation rate was drastically enhanced with respect to all raw and the Zn(II)-exchanged clinoptilolite and even bulk ZnO. In the bulk ZnO sample, aggregation of ZnO active centers caused the lesser absorption of the arrived photons. Thus, lesser reactive species including the e/h pairs, and the above-mentioned radicals can be produced. In general, the bulk sample such as bulk ZnO the path length for travelling the photoinduced e/h pairs from bulk to the surface of the semiconductor has been increased which results in the e/h recombination. Thus when

ZnO has supported on the surface of both CP and CNP, its photocatalytic activity was increased, because decrease the aggregation of ZnO centers. Besides, zeolites have a permanent internal electric field that can cause higher separation of e/h pairs in the photoexcitedZnO species (Koc et al. 2016; Millot et al. 2004). In the case of CNP, higher photodegradation rate can be also related to the higher effective surface area (Chahkandi et al. 2019; NorouziEsfahani et al. 2020).

Fig. 5B shows that when the supported ZnO-CNP the amount of loaded ZnO was changed. No considerable change in the rate of DCA photodegradation was observed. At higher loading some partial aggregation between ZnO species may be happened and thus only the outer layers of the ZnO aggregates participate in the photon absorption. Based on the observed results, the CZ2 catalyst was used for the next steps.

3.2.3.Effects of catalyst dosage and the pollutant concentration

The results in Fig. 5C and Table 3 show that when the concentration of DCA was increased from 5 to 15 mg/L its photodegradation rate was increased in the applied conditions and thereafter was decreased. However, the collision probability between the photoinduced reactive species (the e/h pairs, superoxide and hydroxyl radicals) and the pollutant molecules plays a key role in the photodegradation rate. This is due to the very short lifetime of these reactive species (about a few nano seconds) and their fast participate in the side effect reactions if no enough molecules of the pollutant present near the catalyst surface, where these reactive species produced. The collision probability depends on the concentration of the pollutant and by increase in its value to a definite level collision probability can increase. Here, this optimum value is 15 mg/L. At higher concentrations, despite of the high collision probability between the above-mentioned speciesthe screening effects of the high concentration of the DCA molecules caused to lesser photons reach the catalyst surface. Thus, the production of the above-mentioned reactive species was decreased that followed the decrease in the degradation rate (TalatMehrabad et al.2019; Nezamzadeh-Ejhieh et al. 2011).

In the next step, the effects of the change in the dose of the CZ2 catalyst in the photodegradation rate of DCA were studied. The results in Fig. 6A and Table 3 confirm that by increase in the CZ2 dose from 0.5 to 0.75 g/L, the photodegradation rate of DCA was increased and after this optimum value, the photodegradation rate was decreased. The increased dose from 0.5 to 0.75 g/L provided more active ZnO center to be countered with photons. Thus more reactive species produced in this range causing the increase in the photodegradation rate. At higher doses beyond this optimum value, the light scattering effects caused to reach lesser photons in the inner parts of the suspension. Thus, the photoexcitation of ZnO was decreased. Further, at higher doses, aggregation of the solid particles was increased. The resulted decrease in the effective surface area caused also the decrease in the photoexciation of the ZnO species (Zebardast et al. 2018; Movahedi et al. 2009) Thus, at higher dosages above 0.75 mg/L the photodegradation rate was decreased.

3.2.4.Effect of the solution pH

One the most important key operating variable on the photodegradation yield of a general heterogeneous photocatalysis is the solution pH. This factor simultaneously affects the charges aggregated on the surface of the catalyst and the various ionic species for the molecules of the pollutant present in the media. The presence of such charged species in whole of the media results in the electrical attraction or repulsive forces that drastically determine the overall photodegradation efficiency (Senobari et al. 2018).

Thus the effects of the change in solution pH were evaluated by testing some photodegardation experiments in various pH ranging from the acidic to alkaline pHs. The resulted Hinshelwood plots are shown in Fig. 6B and the obtained rate constants in Table 3. The results show that the best DCA photodegradation rates obtained in the relatively acidic pHs of 5-6.

In section 3.1.4,the pHpzc about of 7.1 was obtained for the CZ2 catalyst. At this pH the surface of the CZ2 catalyst has a net zero charge. At pHs below this value the surface of CZ2 catalyst has a net positive charge. In contrast, at acidic pHs about 3, more DCA molecules have protonated because the conjugated acid of DCA has apKa-value of 2.97. Thus, in acidic pHs about 3, a repulsive force has resulted due to the repulsive force between these positively charged species. By increasing in pH towards 5-6, more DCA molecules are present as the neutral form while the surface of the CZ2 catalyst has positively charged yet. Thus, an attraction force can form between the positive charges accumulated on the catalyst surface and free electrons on the nitrogen atoms of neural DCA molecules in this pH range caused to higher rate for DCA photodegradation. When pH of solution was increased to pHs above the pHpzc, the charge on the surface of the catalyst changes to negative. In these pHs, a repulsive force between the free electron pairs on DCA molecules and the negatively charged surface. Thus, the photodegradation rate of DCA was decreased by increasing in pH toward the stronger alkaline pHs. Detailed discussion on the various effects of solution pH on the photodegradation efficiency has been illustrated in the literature (Bunluesak et al. 2020; Nezamzadeh-Ejhieh et al. 2010).

3.2.5. HPLC study

We used HPLC technique for confirming the DCA photodegradation. Thus, some photodegradation experiments were performed based on the optimal parameters at two photodegradation times of 180 and 30 min.The resulted phodegradaded solutions were separated by the centrifugation and injected to the HPLC column. Such HPLC analysis was also applied on the blank DCA solution. The obtained HPLC chromatograms are shown in Fig. 7 that show a sharp peak for the blank DCA solution at retention time about 2.87 min. The intensity of this peak was drastically decreased after the photodegradation for 180 min and 300 min. The decrease in the peak intensities showed that 74% and 87% of DCA molecules were degraded during these times, respectively. Further, new weak peaks formed at retention time of 2.45 min were appeared that belong to formation of the degradation intermediates. This intermediate was further degraded by elongation of the process, because its intensity was decreased during time. No further investigation done to detect degradation intermediates in this step and only HPLC was used for confirming the DCA photodegradation.

Conclusion

Clinoptilolite nanoparticles (CNPs) were successfully prepared by the mechanical ball-mill process. ZnO was supported on the CNP via the ion-exchange and calcination processes. pHpzc of the ZnO-CNP samples with various loadings of ZnO did not changed from 7.1, confirming that the surface of CNP covered by a ZnO layer and this layer controls the accumulated charges on the surface. No considerable change in the bandgap was also observed by the change in the ZnO loading. The kinetics of the photodegradation process obeyed the apparent first order kinetic model by applying the Hinshelwood model. The best photodegradation rate was achieved in moderate acidic pH about 5–6 in which the DCA is present in the neutral form and the catalyst surface has a net positive charge.

Declarations

Acknowledgement

The authors thank Mohammad Alizadeh and Mohammad HosseinKazemzadeh for performing instrumental analysis of the samples, as experts in laboratory analysis in Shahreza Branch, Islamic Azad University, Isfahan, Iran. The authors also thank the university president for supporting this work.

-Ethical Approval: **Not applicable**

-Consent to Participate: **Not applicable**

-Consent to Publish: **All authors are agree to publish**.

-Authors Contributions:

AlirezaNezamzadeh-Ejhieh: Conceptualization, Methodology, Supervision, Software, Writing- Reviewing and Editing, Validation, **Formal analysis, Supervision,**

Fereshtehlazdani: Data curation, Writing- Original draft, Visualization, Investigation, **Resources, Investigation**

-Funding: **Not applicable**

-Competing Interests: **Not applicable**

-Availability of data and materials: **Not applicable**

References

Aghdasi S, Shokri M (2016), Photocatalytic degradation of ciprofloxacin in the presence of synthesized ZnOnanocatalyst: The effect of operational parameters, Iran. J. Catal. 6(5):481-487.

Ahmad Bhat Sh, Zafar F, Hossain Mondal A, Abdul Kareem, UllahMirza A, Khan Sh, Mohammad A, RizwanulHaq Q, Nishat N(2020), Photocatalytic degradation of carcinogenic Congo red dye in aqueous solution, antioxidant activity and bactericidal effect of NiO nanoparticles, J. Iran. Chem. Soc. 17:215–227.

Akyuz M, Ata S(2006), Simultaneous determination of aliphatic and aromatic amines in water and sediment samples by ion-pair extraction and gas chromatography–mass spectrometry, J. Chromatogr. A. 1129 :88–94.

Arabpour N, Nezamzadeh-Ejhieh A (2015), Modification of clinoptilolitenano-particles with iron oxide: Increased composite catalytic activity for photodegradation of cotrimaxazole in aqueous suspension, Mater. Sci. Semicond. Proces. 31: 684–692.

Arunkumar M, Samson Nesaraj A(2020), Photocatalytic degradation of malachite green dye using NiAl2O4 and Co doped NiAl2O4 nanophotocatalysts prepared by simple one pot wet chemical synthetic route, Iran. J. Catal. 10 (3): 235-245.

Assi N, Tehrani M S, AberoomandAzar P, Husain Syed W(2017), Microwave-assisted sol–gel synthesis of $Fe_{2.9}O_4$/ZnO core/shell nanoparticles using ethylene glycol and its use in photocatalytic degradation of 2-nitrophenol, J. Iran. Chem. Soc. 14: 221–232.

Azimi S, Nezamzadeh-Ejhieh A (2015), Enhanced activity of clinoptilolite-supported hybridized PbS–CdS semiconductors for the photocatalytic degradation of a mixture of tetracycline and cephalexin aqueous solution, J. Molecul. Catal. A: Chem. 408 :152–160.

Balakrishnan M, John R(2020), Properties of sol-gel synthesized multiphase TiO2 (AB)-ZnO (ZW) semiconductor nanostructure: An effective catalyst for methylene blue dye degradation, Iran. J. Catal. 10(1): 1-16.

Behin J, Ghadamnan E, Kazemian H (2019), Recent advances in the science and technology of natural zeolites in Iran, Clay Minerals 54 :131-144.

Bindu P, Thomas S(2014), Estimation of lattice strain in ZnO nanoparticles: X-ray peak profile analysis, J. Theoretical Appl. Phys. 8: 123–134.

Bordbar M, Forghani-pilerood S, Yeganeh-Faal A(2016), Enhanced photocatalytic activity of sonochemical derived ZnO via the co-doping process, Iran. J. Catal. 6(5): 415-421.

Bordbar M, Vasegh Seyed M, Jafari S, YeganehFaal A(2015), Optical and photocatalytic properties undoped and Mn-doped ZnO nanoparticles synthesized by hydrothermal method: Effect of annealing temperature, Iran. J. Catal. 5(2): 135-141.

Bunluesak Th, Phuruangrat A, Teppetcharat J, Patiphatpanya P, Dumrongrojthanath Ph, Thongtem S, Thongtem T(2020), Enhanced visible-light-driven Pd/Bi_2WO_6 heterojunctions used for photodegradation of rhodamine B, J. Iran. Chem. Soc. 2020 https://doi.org/10.1007/s13738-020-02095-7.

Chahkandi M, SaadatdarArami Seyedeh R, Mirzaei M, Mahdavi B, Hosseini-Tabar Seyed M (2019), A new effective nano-adsorbent and antibacterial material of hydroxyapatite, J. Iran. Chem. Soc. 16 :695–705.

Derikvandi H, Nezamzadeh-Ejhieh A(2017), Increased photocatalytic activity of NiO and ZnO in photodegradation of a model drug aqueous solution: Effect of coupling, supporting, particles size and calcination temperature, J. Hazard. Mater. 321 629–638.

Derikvandi H, Vosough M, Nezamzadeh-Ejhieh A(2020), A comprehensive study on the enhanced photocatlytic activity of a double-shell mesoporousplasmonic Cu@Cu_2O/SiO_2 as a visible-light driven nanophotocatalyst, Environ. Sci. Pollution Res. 2020 https://doi.org/10.1007/s11356-020-08817-x.

DharmrajKhairnar S, RajendraPatil M, Shankar Shrivastava V (2018), Hydrothermally synthesized nanocrystalline Nb_2O_5 and its visible-light photocatalytic activity for the degradation of congo red and methylene blue, Iran. J. Catal. 8(2) :143-150.

Dianat S(2018), Visible light induced photocatalytic degradation of direct red 23 and direct brown 166 by $InVO_4$-TiO_2nanocomposite, Iran. J. Catal. 8(2) :121-132.

Divband B, Jodaie A, Khatmian M (2019), Enhancement of photocatalytic degradation of 4-nitrophenol by integrating Ag nanoparticles with ZnO/HZSM-5 nanocomposite, Iran. J. Catal. 9 : 63-70.

Eslami A, Oghazyan A, Sarafraz M(2018), Magnetically separable MgFe2O4 nanoparticle for efficient catalytic ozonation of organic pollutants, Iranian J. Catal. 8(2) :95-102.

Faghihian H, Talebi M, Pirouzi M (2008), Adsorption of nitrogen from natural gas by clinoptilolite, J. Iran. Chem. Soc. 5: 394–399.

Ghattavi Sh, Nezamzadeh-Ejhieh A(2019), A brief study on the boosted photocatalytic activity of AgI/WO_3/ZnO in the degradation of Methylene Blue under visible light irradiation, Desal. Water Treat. 166 :92–104.

Giahi M, Hoseinpour Dargahi A(2016), Photocatalytic degradation of phenylephrine hydrochloride in aqueous solutions by synthesized SnO_2-doped ZnO nanophotocatalyst, Iran. J. Catal. 6(4): 381-387.

Habibi M. H, Askari E(2011), Photocatalytic degradation of an azo textile dye with manganese-doped ZnO nanoparticles coated on glass, Iran. J. Catal. 1: 41-44.

Honarmand M, Golmohammadi M, Hafezi-bakhtiari J (2020) Synthesis and characterization of SnO_2 NPs for photodegradation of eriochrome black-T using response surface methodology. Environ Sci Poll Res

(2020) https://doi.org/10.1007/s11356-020-11086-3

Huang Y, Hui Xu, Luo D, Guo Q (2019), Visible light-driven flower-like Bi/$BiOCl_xBr_{(1-x)}$heterojunction with excellent photocatalytic performance, J. Iran. Chem. Soc. 16 2743–275.

Khanmohammadi M, Rahbar Shahrouzi J, Rahmani F (2020) Insights into mesoporous MCM-41-supported titania decorated with CuO nanoparticles for enhanced photodegradation of tetracycline antibiotic. Environ Sci Poll Res (2020) https://doi.org/10.1007/s11356-020-10546-0

Khodadadi B, Bordbar M (2016), Sonochemical synthesis of undoped and Co-doped ZnO nanostructures and investigation of optical and photocatalytic properties, Iran. J. Catal. 6(1): 37-42.

Koc S. O, Koseoglu K, Galioglu S, Akata B, Salamov B G(2016), Effects of pressure and *electricfield* on the charge transport mechanisms in the silver-modified-*zeolite* porous microstructure, MicroporousMesoporous Mater. 223 : 18-26.

Matei E, Enculescu M, Preda N, Enculescu I (2012), ZnO morphological, structural and optical properties control by electrodeposition potential sweep rate, Mater. Chem. Phys. 134 :988-993.

Millot Y, Man P. P, Springuel-Huet M, Fraissard J (2004), Quantification of *electric-field* gradients in the supercage of HY, steam-dealuminated Y and lanthanum-exchanged Y *zeolites* by 129Xe and 131Xe NMR or physisorbed xenon gas, Studies Surf. Sci. Catal. 154, Part B: 1400-1405.

Mohamed JafferSadiq M, Samson Nesaraj A(2014), Reflux condensation synthesis and characterization of Co_3O_4 nanoparticles for photocatalytic applications, Iran. J. Catal. 4(4) :219-226.

Mohammadi V, Tabatabaee M, Fadaei A, Mirhoseini Seyed A(2020), Comparing activated carbon and magnetic activated carbon in removal of linear alkylbenzenesulfonate from aqueous solution by heterogeneous catalytic ozonation process, Iran. J. Catal. 10 (3): 209-218.

Movahedi M**,** Mahjoub A. R**,** Janitabar-Darzi S (2009), Photodegradation of Congo red in aqueous solution on ZnO as an alternative catalyst to TiO_2, J. Iran. Chem. Soc. 6 : 570–577.

Muhammad W, Ullah N, Haroon M, HaiderAbbasi B(2019), Optical, morphological and biological analysis of zinc oxide nanoparticles (ZnO NPs) using Papaversomniferum L. RSC Adv. 9 29541-29548.

Naderpour H, Noroozifar M, Khorasani-Motlagh M(2013), Photodegradation of methyl orange catalyzed by nanoscalezerovalent iron particles supported on natural zeolite, J. Iran. Chem. Soc. 10 :471–479.

Nagaraju G, Udayabhanu, Shivaraj, Prashanth S.A, Shastri M, Yathish K.V, Anupama C, Rangappa D(2017), Electrochemical heavy metal detection, photocatalytic, photoluminescence, biodiesel production and antibacterial activities of Ag–ZnO nanomaterial, Mater. Res. Bull. 94 :54–63.

Nezamzadeh-Ejhieh A, Salimi Z (2011), Solar photocatalytic degradation of o-phenylenediamine by heterogeneous CuO/X zeolite catalyst, Desalination 280 : 281-287.

Nezamzadeh-Ejhieh A, Zabihi-Mobarakeh H(2014), Heterogeneous photodecolorization of mixture of methylene blue and bromophenol blue using CuO-nano-clinoptilolite, J. Ind. Eng. Chem. 20 :1421–1431.

Ng Y-C (2011), Shamsuddin M, Solid state morphology and band gap studies of ETS-10 supported CdS nanoparticles, J. Iran. Chem. Soc. 8 : S28–S33.

Nosuhi M, Nezamzadeh-Ejhieh A (2018), An indirect application aspect of zeolite modified electrodes for voltammetric determination of iodate, J. Electroanal. Chem. 810 119–128.

Norouzi Esfahani R**,** Khaghani Sh**,** Azizi A**,** Gomarian M (2020), Facile and eco-friendly synthesis of TiO_2 NPs using extracts of *Verbascumthapsus* plant: an efficient photocatalyst for reduction of Cr(VI) ions in the aqueous solution, J. Iran. Chem. Soc. 17 :205-213.

Olad A**,** Khatamian M**,** Naseri B(2011), Removal of toxic hexavalent chromium by polyaniline modified clinoptilolite nanoparticles, J. Iran. Chem. Soc. 8 8 S141–S151.

Omrani N, Nezamzadeh-Ejhieh A, Alizadeh M (2019), Brief study on the kinetic aspect of photodegradation of sulfasalazine aqueous solution by cuprous oxide/cadmium sulfide nanoparticles, Desal. Water Treat. 162 :290-302.

Palma T. L, Vieira B, Nunes J, Lourenço J. P, Monteiro O. C, Costa M. C(2020), Photodegradation of chloramphenicol and paracetamol using PbS/TiO_2 nanocomposites produced by green synthesis, J. Iran. Chem. Soc. 2020, https://doi.org/10.1007/s13738-020-01906-1.

Pande U.C, Dwivedi A.H(2011), Methylene blue sensitized photodechlorination of isomeric mono- and dichloroanilines via molecular complex formation mechanism, E-J. Chem. 8: 1086-1093.

Pouretedal H. R, Fallahgar M, Pourhasan F. S, Nasiri M(2017), Taguchi optimization of photodegradation of yellow water of trinitrotoluene production catalyzed by nanoparticles TiO_2/N under visible light, Iranian J. Catal. 7(4) :317-326.

Pouretedal H. R, Sohrabi A. M (2016), Photosensitization of TiO_2 by ZnS and bromothymol blue and its application in photodegradation of para-nitrophenol, J. Iran. Chem. Soc. 13: 73-79.

Rahimi B, Jafari N, Abdolahnejad A, Farrokhzadeh H, Ebrahimi A(2019), Application of efficient photocatalytic process using a novel BiVO/TiO_2-NaY zeolite composite for removal of acid orange 10 dye in aqueous solutions: Modeling by response surface methodology (RSM), J. Environ. Chem. Eng. 7: 103253.

Rappoport Z.Z (2007) , The Chemistry of Anilines: Part 1. The Chemistry of Functional Group Series, Wiley, New York.

Rashmi B.N, Harlapur Sujatha F, Avinash B, Ravikumar C.R, Nagaswarupa H.P, Anil Kumar M.R, Gurushantha K, Santosh M.S(2020), Facile green synthesis of silver oxide nanoparticles and their electrochemical, photocatalytic and biological studies, Inorg. Chem. Commun. 111: 107580.

Rostami-Vartooni A, Moradi-Saadatmand A, Bagherzadeh M, Mahdavi M(2019), Green synthesis of $Ag/Fe_3O_4/ZrO_2$nanocomposite using aqueous Centaureacyanus flower extract and its catalytic application for reduction of organic pollutants, Iran. J. Catal. 9: 27-35.

Segundo I. R, Freitas E, Landi Jr. S, Costa Manuel F. M, Carneiro J. O, Smart(2019), Photocatalytic and Self-Cleaning Asphalt Mixtures: A Literature Review, Coatings 9 696 (1-22 pages) doi:10.3390/coatings9110696.

Senobari S, Nezamzadeh-Ejhieh A(2018), A p-n junction NiO-CdS nanoparticles with enhanced photocatalytic activity: A response surface methodology study, J. Molecul. Liq. 257 :173–183.

Shabani L, Aliyan H(2016), Synthesis and photocatalytic activity of nanosized modified mesocellulous silica foams (MCFs) with PW12 and vanadium oxide, Iran. J. Catal. 6(3): 221-228.

Shah S, Hao C (2016) Density functional theory study of direct and indirect photodegradation mechanisms of sulfameter. Environ Sci Poll Res 23: 19921-19930

Shahwan T, Zünbül B, Tunusoğlu O, Eroğlu A. E(2005), AAS, XRPD, SEM/EDS, and *FTIR* characterization of Zn2+ retention by calcite, calcite–kaolinite, and calcite–*clinoptilolite* minerals, J. Colloid. Interf. Sci. 286 :471-478.

Sharifian S, Nezamzadeh-Ejhieh A(2016), Modification of carbon paste electrode with Fe(III)-clinoptilolite, nano-particles for simultaneous voltammetric determination of acetaminophen and ascorbic acid, Mater. Sci. Engin. C, 58: 510–520.

Sobhani-Nasab A, Eghbali-Aranib M, Hosseinpour-Mashkani Seyed M, Ahmadi F, Rahimi-Nasrabadi M, Ameri V(2020), Eco-friendly preparation and characterization of CuMn2O4 nanoparticles with the green capping agent and their photocatalytic and photovoltaic applications, Iran. J. Catal. 10 (2): 91.

SowriBabu K, Ramachandra Reddy A, Sujatha Ch, Venugopal Reddy K, Mallika A. N(2013), Synthesis and optical characterization of porous ZnO, J. Adv. Ceram. 2: 260–265.

TalatMehrabad J, Partovi M, Arjomandi Rad F, Khalilnezhad R(2019), Nitrogen doped TiO2 for efficient visible light photocatalytic dye degradation, Iran. J. Catal. 9(3) :233-239.

Thirumalai K, Balachandran S, Swaminathan M (2016), Superior photocatalytic, electrocatalytic, and self-cleaning applications of Fly ash supported ZnOnanorods, Mater. Chem. Phys. 183 :191-200.

Vafayi L, Gharibe S(2015), Enhancement of photocatalytic activity of ZnO–SiO_2 by nano-sized Pt for efficient removal of dyes from wastewater effluents, Iran. J. Catal. 5(4):365-371.

Yousefi F, Nezamzadeh-Ejhieh A (2020), Photodegradation of phenazopyridine in an aqueous solution by CdS-WO_3nanocomposite, Desal. Water Treat. 182 :299-308.

Yuonesi M, Pakdel A (2010), Effect of low concentration of nickel on structural and optical properties of ZnO nanofilms, Physica B 405: 2083–2087.

Zebardast M, FallahShojaei A, Tabatabaeian Kh (2018), Enhanced removal of methylene blue dye by bimetallic nano-sized MOF-5s, Iran. J. Catal. 8(4) :297-309.

Zh B, Lin S(2009), Effects of 3,4-dichloroaniline on testicle enzymes as Biological markers in rats, Biomed. Environ. Sci. 22: 40-43.

Figures

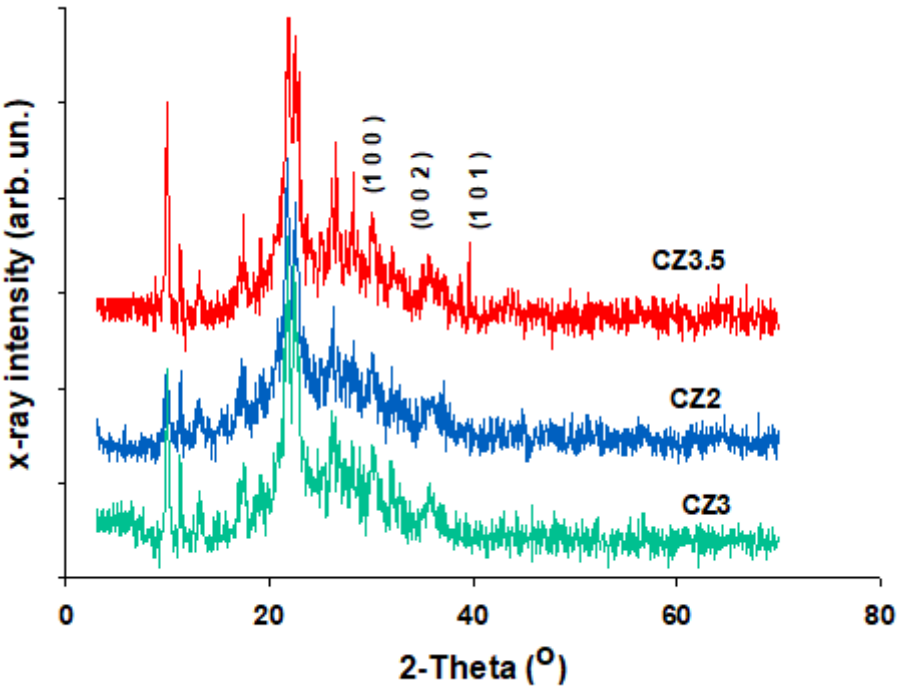

Figure 1

(A) XRD patterns of the various ZnO-CNP samples.

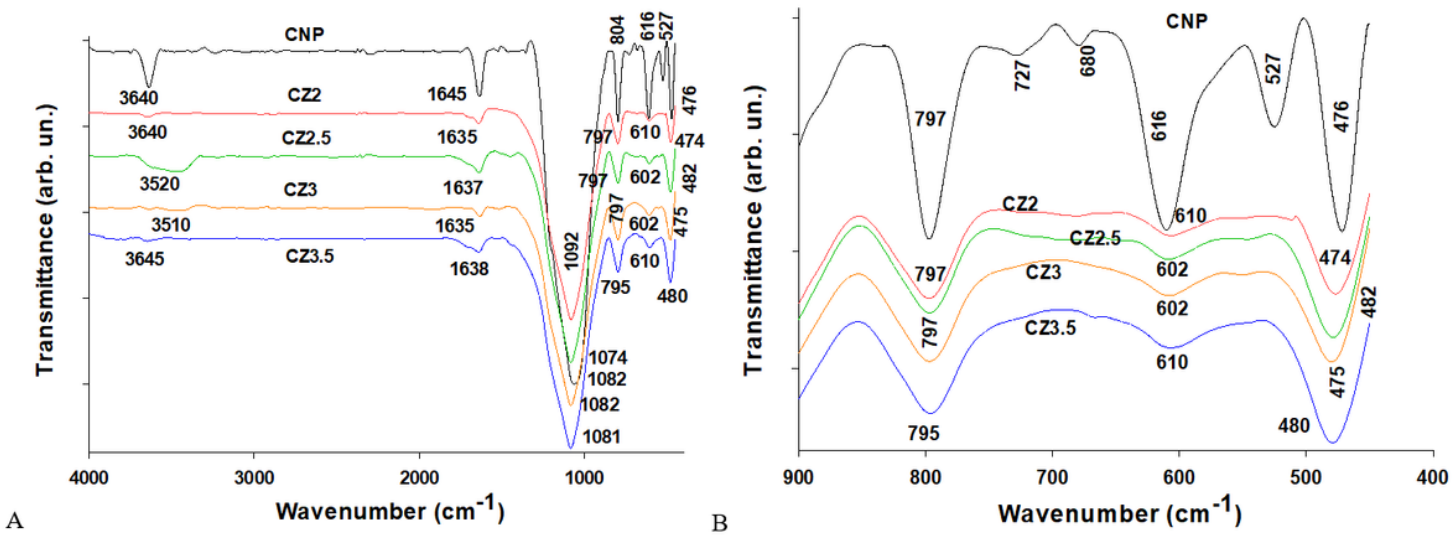

Figure 2

FTIR spectra of the raw CNP and ZnO-loaded samples (A) and the scaled spectra in the range of 900-400 cm-1 (B).

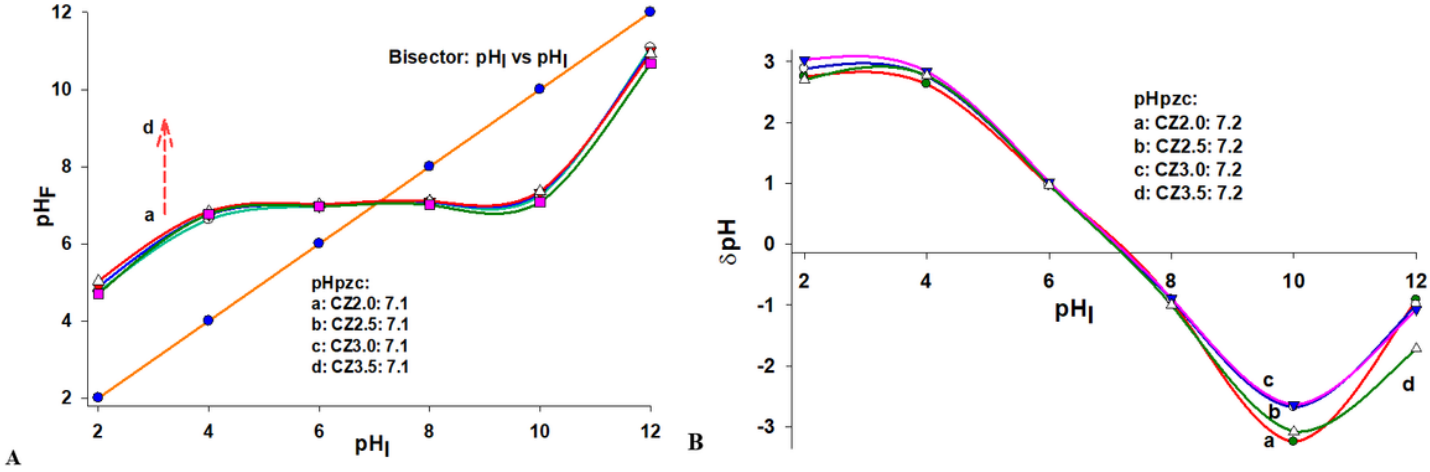

Figure 3

The plots used for the estimation of pHpzc of ZnO-CNP samples.

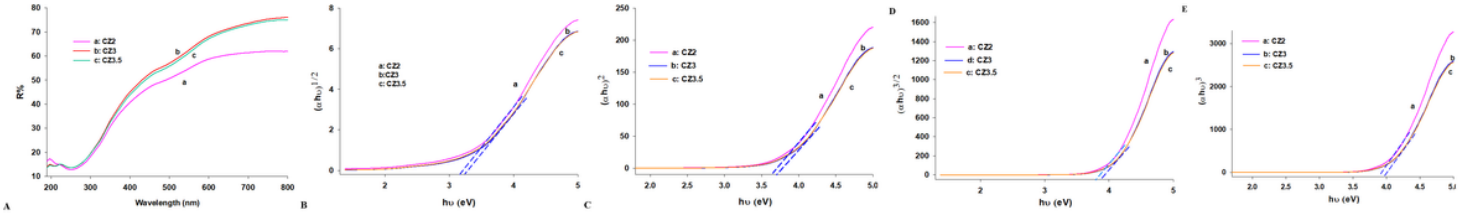

Figure 4

Reflectance spectra of the ZnO-CNP samples with different ZnO-loaded obtained in DRS study (A) and typical Tauc plots resulted from the reflectance spectra (B-E).

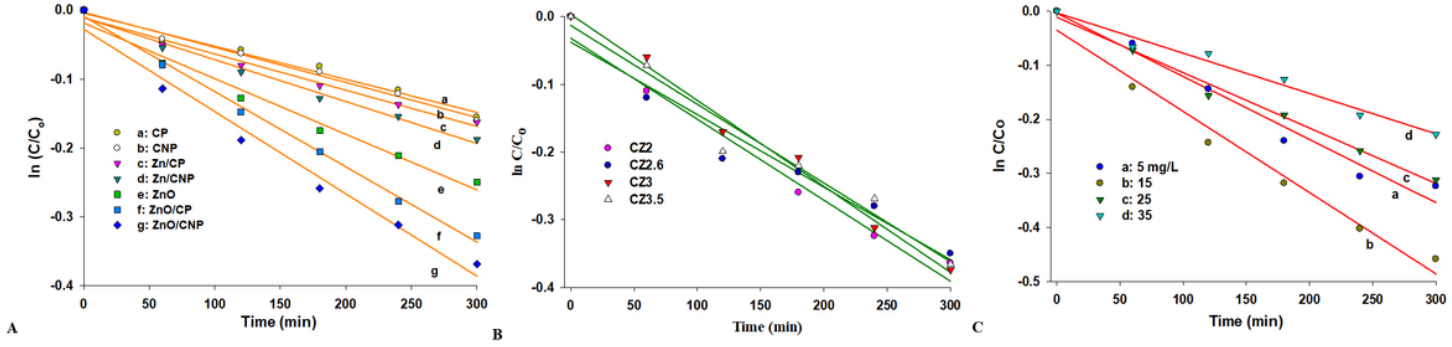

Figure 5

(A) Typical Hinshelwood plots for the effect of the loaded ZnO onto the CNP structure and other samples; conditions in all cases: CDCA =5 ppm at pH 5.8, 0.1 g/L of the catalyst (CZ2 catalyst); (B) The effects of the extent of ZnO-loading on the activity of ZnO-CNP samples (CDCA =5 ppm at pH 5.8, 0.1 g/L of the catalyst); (C) The effects of the DCA concentration on the activity of ZnO-CNP samples (0.1 g/L of the CZ2 catalyst).

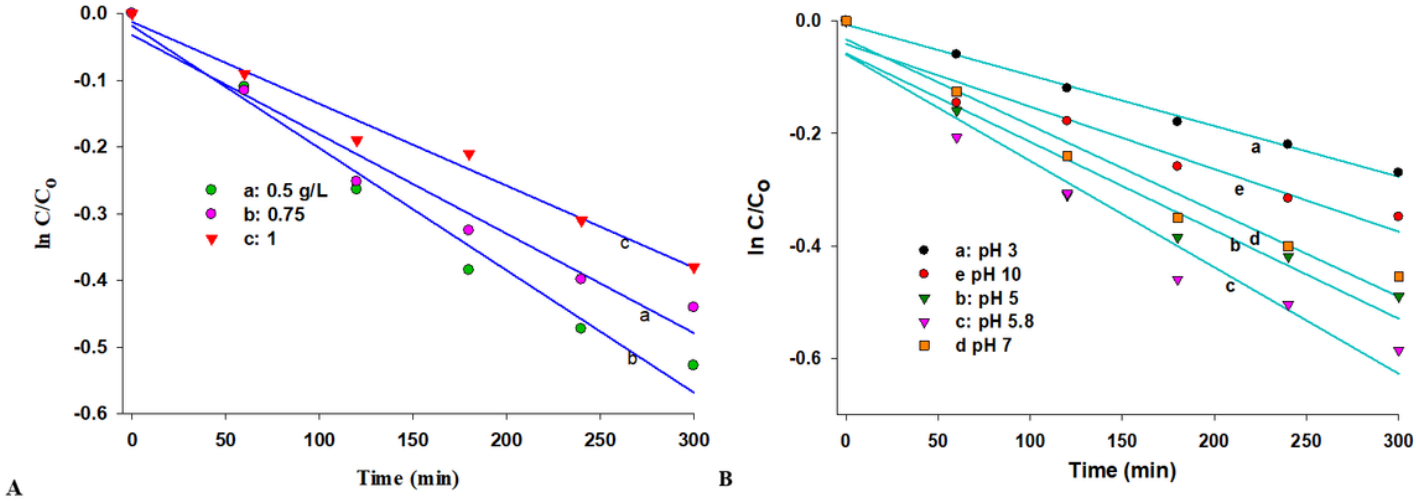

Figure 6

Typical Hinshelwood plots for (A) the effect of the dose of the CZ2 catalyst (CDCA = 15 ppm at pH 5.8); (B) the effect of the solution pH (the catalyst dose = 0.75 g/L, CDCA = 15 ppm).

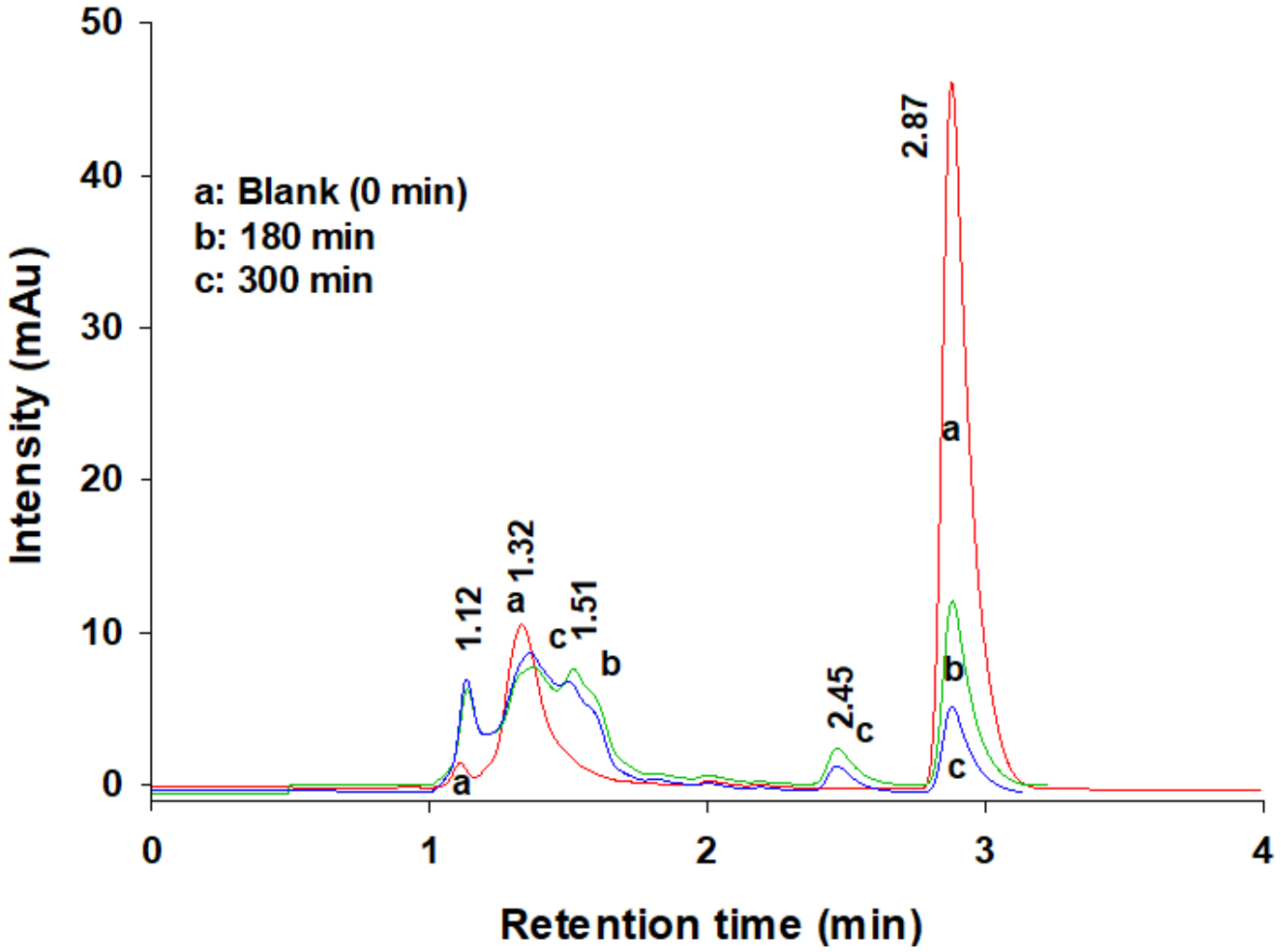

Figure 7

HPLC chromatograms of DCA solutions during different photodegradation times of (a) 0 min, (b) 180 min and (c) 300 min, Photodegradation conditions: CDCA = 15 ppm at pH 5.8, catal. dose: 0.5 g/L; HPLC conditions: Column: C18, Reverse phase, Moble phase: 70:30 v acetonitrile/water, UV detector at 254 nm.